International Journal of Research in Engineering, Science and Management
Volume-2, Issue-8, August-2019
www.ijresm.com | ISSN (Online): 2581-5792

Photomineralization of Methyl Orange and Phenol by Peroxymonosulfate Activated Heterogeneous of $CoFe_2O_4$ Ferrite: A Comparative Study

M. Srinivas
Department of Chemistry, Atria Institute of Technology, Bangalore, India

***Abstract*: $CoFe_2O_4$ sample was prepared by sol-gel combustion method. The prepared samples were characterized by powder X-ray diffraction (PXRD), UV-Vis absorbance spectra, Fourier Transform Infrared spectroscopy, (FTIR). $CoFe_2O_4$ was utilized as a photo catalyst under visible light irradiation. Further studies showed that $CoFe_2O_4$ has a higher catalytic function in the presence of peroxymonosulphate (PMS), in presence of $CoFe_2O_4$ capable of catalyzing the degradation of Methyl orange (MO) and phenol. Higher photocatalytic activity shown at pH 7 compared to pH 3 and 10 respectively. Photocatalytic reaction mechanism was investigated by analyzing the data obtained.**

***Keywords*: Spinel structure, Photocatalysis, semiconductor, Adsorption, Peroxy monosulphate.**

1. Introduction

Semiconductor photo catalysis has been widely used for the treatment of polluted water. There have been many reports that various organic pollutants can be degraded completely through photo catalysis using metal oxide semiconductors or their hetero-architectures under ultraviolet light irradiation [1]-[3]. Ferrites are viable alternative materials to TiO_2 to be used as photo catalysts for hydrogen production; transition metal ferrites have a number of advantages, mainly emphasizing their low cost, effective catalytic activity, corrosion resistance and most importantly their wide band gap into the visible light spectrum. Among various semiconducting materials $CoFe_2O_4$ ferrite is a class of semiconductors with narrow band gap, good photochemical stability, favourable magnetic property and exhibits characteristic visible-light response [4]-[6]. Spinels with only divalent ions in tetrahedral sites are called normal, while compounds with the divalent ions in the octahedral sites are called inverse. In the inverse spinel structure, all the Co^{2+} ions occupy the octahedral sites of lattice structure, half of the Fe^{3+} ions also occupy the same sites and the rest of the Fe^{3+} ions stay in tetrahedral sites [7]. The ferrite spinel structure is based on a closed-packed oxygen lattice, in which tetrahedral (called A sites) and octahedral (called B sites) interstices are occupied by the cations. The selection of these materials is based on the redox activity and especially their ability to store oxygen in its crystalline lattice. Ferrites have a tendency when burned under reducing atmospheres to form compounds with oxygen defects, which facilitates the fixation of oxygen in the existing vacancies. Therefore, these materials are excellent candidates for the production of hydrogen from water under solar illumination. It is well known that bivalent cation (Co^{2+}) and trivalent ferric ion (Fe^{3+}) can distribute at both tetrahedral and octahedral sites and this type of cationic distribution affects the magnetic properties of spinel ferrite [8],[9]. The presence of $CoFe_2O_4$ magnetic nanoparticles enhances the efficiency of the degradation of organic contaminants and can be easily separated magnetically. The main goal of in this work is to synthesis of $CoFe_2O_4$ by solution sol-gel combustion route method and to probe its photocatalytic activity under visible light irradiation

2. Experimental

A. *Materials*

The Methyl Orange (MO) dye and phenol was obtained from Sigma Aldrich. Ferrous sulfate, cobalt sulfate and ethanol were supplied from Nice chemicals. Oxone ($2KHSO_5 \cdot KHSO_4 \cdot K_2SO_4$) was obtained by Avra synthesis Pvt. Ltd. Sodium hydroxide (NaOH) and hydrochloric acid (HCl) were from Sisco-chemical industries. All chemicals were analytic grade reagents and used without further purification. Double distilled water was used in all the experiments.

B. *Synthesis of $CoFe_2O_4$ by sol gel route combustion method*

Ferrite compound of the type $CoFe_2O_4$ were synthesized by the sol–gel auto-combustion reaction method. The analytical grade $Fe(NO)_3 \cdot 9H_2O$, $Co(NO)_3 9H_2O$ and citric acid ($C_6H_8O_7 \cdot H_2O$) were used as raw materials. The stoichiometric amount of nitrates and citric acid was first dissolved in distilled water to form a clear solution. The molar ratio of nitrates to citric acid was 1: 1. The solution was evaporated by stirring and heating for 4 hours at 70 °C further, heated to 90 °C until turned into a gel. Finally, the product was calcined in a furnace for 2 hours at 800°C.

C. Catalyst characterization

The powder X-ray diffraction (PXRD) patterns were recorded using Bruker D8 Advanced diffractometer, which was operated at 30 kV and 20 mA using Cu Kα with nickel filter. The scan rate was varied from 2°to 0.5°/min to get X-ray diffraction line broadening. The Fourier transform infra-red (FTIR) spectra were obtained using Bruker model Alpha–IR spectrometer with diamond ATR cell. The absorbance spectra were obtained using UV-vis absorbance spectra were recorded in the wavelength range of 200 to 800 nm (Schimadzu-UV 3101 PC UV–Vis-NIR) with $BaSO_4$ as the reference standard.

D. Photochemical reactor

The detail pertaining to photocatalytic degradation experiments are given elsewhere [10]

3. Results and Discussion

A. PXRD studies

PXRD pattern of $CoFe_2O_4$ particle with diffraction peaks of $CoFe_2O_4$ are shown in the Figure 1. The PXRD pattern of $CoFe_2O_4$ shows peaks at 18.35º (111), 30.15º (220), 35.35º (311), 37.42º (222), 43.33º (400), 54.97º (422), 57.36º (511), 62.93º (440) 71.41º (622) 74.53º (533) and in accordance with spinel structure with space group fd-3m which is in agreement with JCPDS standard card (22-1086). The average crystallite size was calculated highest base peak at (311) by using the Scherrer's equation, crystallite size of $CoFe_2O_4$ was found to be 50.52nm.

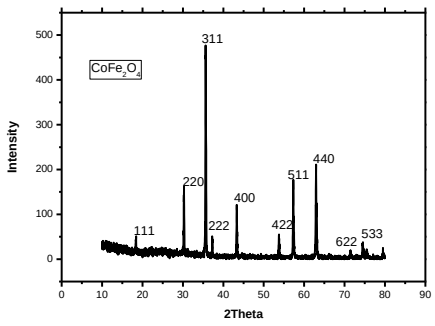

Fig. 1. PXRD pattern of $CoFe_2O_4$

B. UV-visible spectroscopy

UV-Visible spectra of $CoFe_2O_4$ exhibits wide band gap in the range of 350-800 nm. The absorbance range extends from UV light to solar light region explains the photocatalytic efficiency of these materials under solar light has shown in Figure 2 [11-14]. The band gap values were determined from these spectra by converting the absolute absorption values to Kubelka-Munk function F (R∞). The plot of kubelka Munka function $[F(R)hv]^{1/2}$ versus photon energy in electron volts (eV). The band gap of $CoFe_2O_4$ calculated and was found to be 1.68eV**.** The d-d transitions that the metal having d-electrons to transfer between t_2g to eg (Oh) or eg to t_2g (td), these spectra clearly show that values of the energy of the forbidden band are within the visible light spectrum. Electronic configuration Co^{2+} having unpaired d-electrons and these unpaired electrons are excited under illumination of light.

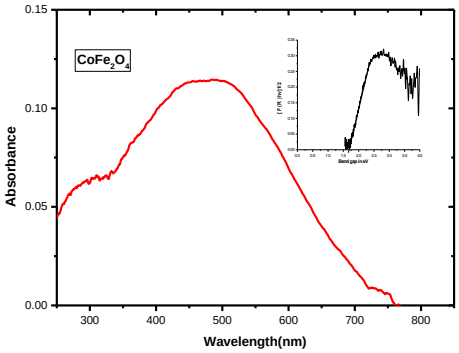

Fig. 2. UV-visible absorbance spectrum of $CoFe_2O_4$

C. FTIR

FTIR spectra of $CoFe_2O_4$, the peak at 577cm^{-1} corresponds to the intrinsic stretching vibrations of both at tetrahedral (Co-O) and octahedral group (Fe-O). This confirms presence of characteristic peak of spinel structure as shown in the Figure.3.

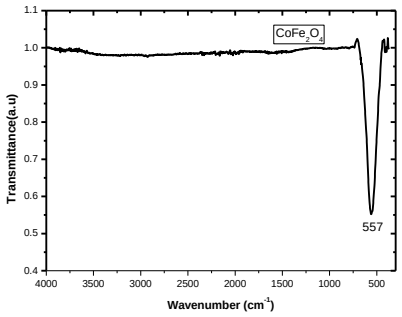

Fig. 3. FTIR spectrum of $CoFe_2O_4$

D. BET

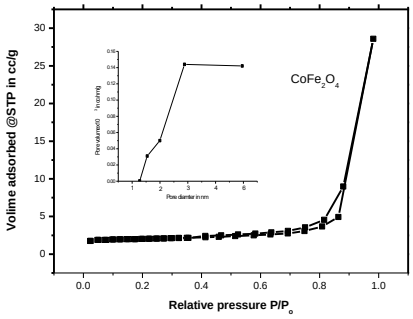

Fig. 4. The N_2 adsorption–desorption isotherm $CoFe_2O_4$. Inset figure shows BJH pore size distribution curve

The specific surface area and pore volume of $CoFe_2O_4$ sample were determined by BET method as shown in Figure.

The pore size distribution is 1.3-6 nm, specific surface area and total pore volume were found to be 6.202 m^2 g^{-1} and 0.0031ccg^{-1} as shown in the Figure 4. BET surface area $CoFe_2O_4$ photocatalyst provides a larger adsorption site on the catalyst surface for phenol and MV thereby shows photocatalytic activity.

E. XPS

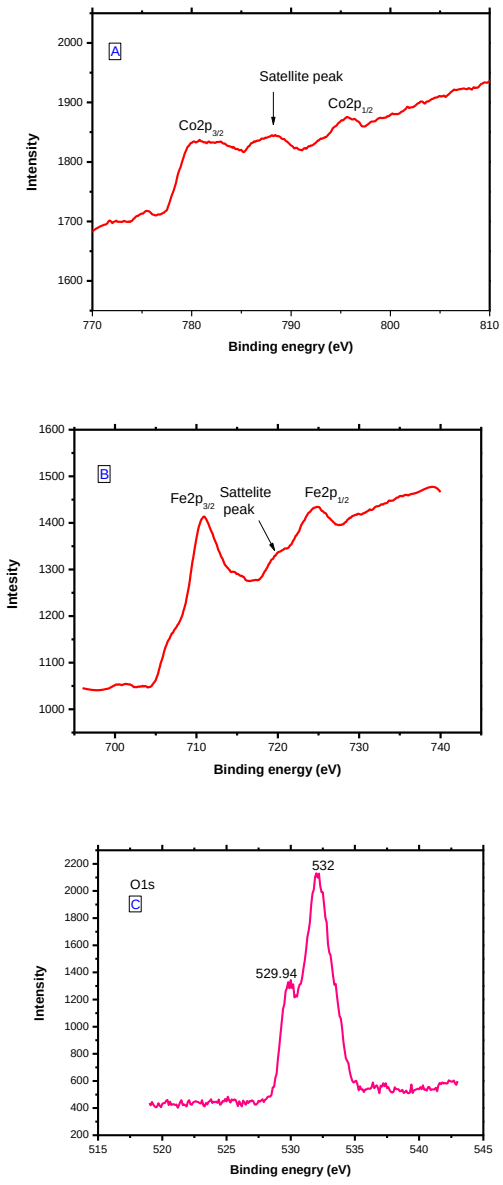

Fig. 5. XPS of $CoFe_2O_4$ showing A) Co 2p, B) Fe 2p and C) O1s peaks

XPS spectrum Co2p in $CoFe_2O_4$ shows two major peaks with binding energy values at 795.79, 788.18 and 780.95eV, corresponding to the $Co2p_{1/2}$ and $Co2p_{3/2}$ spin-orbit peaks respectively of the Co-O phase. The $Fe2p_{3/2}$ and $Fe2p_{1/2}$ states were observed in the 710.89 and 724.72eV. The peak in the range of 710-711eV is attributed to the Fe^{3+} cation located at the octahedral site in the spinal structure. The peak range of 724.72 is endorsed to the Fe^{2+} cation located at the tetrahedral site in the spinal structure. The O1s spectrum shows the existence of oxygen with binding energies at 530.95eV that can be assigning to the lattice-oxygen and the oxygen-deficient regions respectively. The peak observed close to 532.04eV of $CoFe_2O_4$ of O1s spectra indicate the presence of –OH species adsorbed on the surface to the sample (Figure 5). These results indicates that the presence of chemical composition of $CoFe_2O_4$.

F. Adsorption MO and Phenol

Photocatalytic properties have been dependent on the adsorption and transportation of electron-hole pairs [15]-[18]. Adsorption of MO and phenol was studied by using 100mg $CoFe_2O_4$ catalyst at room temperature in the dark. The effect of $CoFe_2O_4$ concentration on the adsorption capacity as shown in Figure 6a and 6b adsorption behaviour of MO and phenol on catalyst follow Langmuir model. Phenol uptake capacity in presence of $CoFe_2O_4$ slightly increases compared to MO. The adsorbed quantities MO and phenol q_t (mg/g $_{catalyst}$), at time t are calculated according to Equation.

$$q_t = \frac{C_o - C_t \times 1000 \times M_w \times V_o}{W_{catalyst}} \quad (1)$$

Where, C_o and C_t (ml/L) are the initial concentrations and concentration at time t of MO respectively, M_w molecular weight of MO (g/mol), V_o is the volume of aqueous dye solution (ml) and $W_{catalyst}$ is the mass of the catalyst (g).

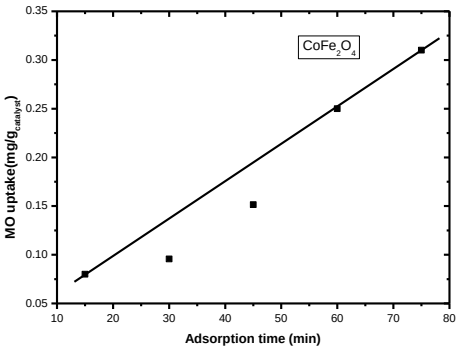

Fig. 6(a). Effect of $CoFe_2O_4$ on MO adsorptivity

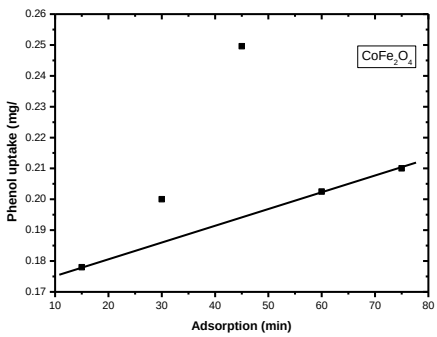

Fig. 6(b). Effect of $CoFe_2O_4$ on phenol adsorptivity

In present work, evaluated by using experimental data from linear transform (t/q_t) = f (t) in Figure 7a and 7b. Hence, adsorption capacities at equilibrium (q_e) at time t are calculated from the slope and adsorption rate constant (k_{ads}) values are calculated intercept of the plot and as shown in the Table 1. The amount of phenol is best adsorptivity than MO.

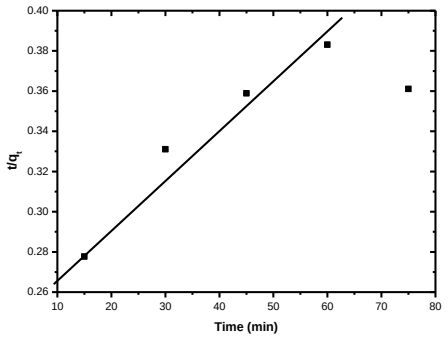

Fig. 7(a). Pseudo- second –order kinetic plot of MO removal

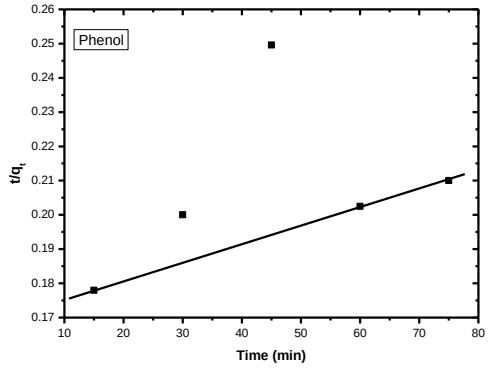

Fig. 7(b). Pseudo- second –order kinetic plot of phenol removal

Table 1
Adsorption study of MO and phenol in absence of light (catalysts dosage = 100 mg)

Photo catalyst	Pollutants	q_e(mg/g $_{catalyst}$)	K_{ads}(g/mg min)
$CoFe_2O_4$	MO	68.96	0.0145
$CoFe_2O_4$	Phenol	207.46	1.0496

G. Photocatalytic Mechanism

$CoFe_2O_4$ particles under solar light illumination generates the holes and electrons, water molecules ionizes to hydroxide ion, oxygen molecule traps the electrons to form super oxide radical, transfer of holes to surface hydroxyl ion produce hydroxyl free radicals.

$$MFe_2O_4 + h\upsilon \rightarrow MFe_2O_4(e^-) + MFe_2O_4(h^+) \quad (2)$$

$$H_2O \rightarrow H^+ + OH^- \quad (3)$$

$$OH^- + O_2 \rightarrow O_2^{\bullet -} \quad (4)$$

$$MFe_2O_4(h^+) + OH^- \rightarrow MFe_2O_4 + {}^{\bullet}OH \quad (5)$$

$$MFe_2O_4(h^+) + OH^- + O_2^{\bullet -} + MV \rightarrow H_2O + CO_2 \quad (6)$$

Photocatalytic activity of $CoFe_2O_4$ under visible light illumination for photominaralization of MO and phenol, $CoFe_2O_4$ alone shows photocatalytic activity, the presence of oxidant like PMS enhance the activity. Further activity explored by varying pH parameter viz., 3, 7 and 10. Cobalt (II) ions serves as Lewis acid and capture H_2O to from activated hydroxyl radicals on the surface of $CoFe_2O_4$ and HSO^-_5 bonded in the form of $CoFe_2O_4$-O-H- HSO^-_5 through hydrogen bonds. The Co^{2+} ions transfer electron to break bond the O-H and O-O bonds and oxidized to Co^{3+} with the generation of sulphate radicals

Table 2
Effect of pH 3 on MO and Phenol

Photocatalyst	Pollutants	PMS concentration (ppm)	Rate constant x 10^{-2} min^{-1}	Degradation time (min)
$CoFe_2O_4$	MO	-	2.2447	160
$CoFe_2O_4$	MO	10	2.9529	140
$CoFe_2O_4$	Phenol	-	3.4977	100
$CoFe_2O_4$	Phenol	10	4.7772	80

$$Co^{2+} + HSO_5^- \rightarrow Co^{3+} + SO_4^{\bullet -} + OH^- \quad (7)$$

Effect of pH 3 on MO and Phenol

At pH 3, in presence of $CoFe_2O_4$ (100mg), the degradation of MO takes place around 160 min. Further addition of PMS (Co^{2+}/PMS) activity increases (140min) certain extent. In case of phenol, decomposition takes place around 100min, when the addition of PMS activity increases (80min) as shown in the Figure 8 and Table 2. MO exist as high acidic conditions and it behaves positively charged at this pH, acquires positive charge which gets less adsorbed and in turn less degraded by the positively charged catalyst surface due to columbic repulsion At pH 3 phenol exist as its ptotonated form and it is slightly acidic in nature when compared to MO, phenol also acquires positive charge which gets more adsorbed thereby minimum columbic repulsion takes place and slightly high photocatalytic activity compared to MO.

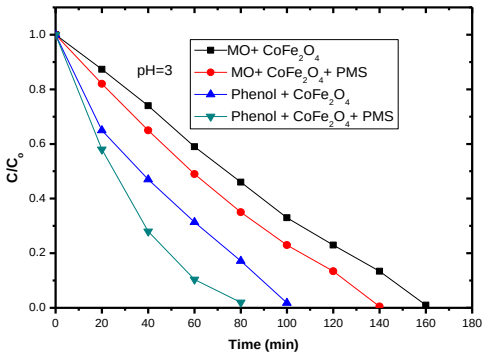

Fig. 8. Effect of pH 3 for the degradation of MO and Phenol

Effect of pH 7 on MO and Phenol

At pH 7, MO and Phenol undergoes decomposition in presence of $CoFe_2O_4$, further addition of PMS activity increases and undergoes complete degradation. At neutral pH MO solution has below PZC, MO anions are readily adsorbed onto the catalyst surface via columbic interaction. Phenol exists in its ionic-form with minimum water solubility and adsorption onto photocatalyst is enhanced hence increased degradation rate

than MO as shown in the Figure 9.

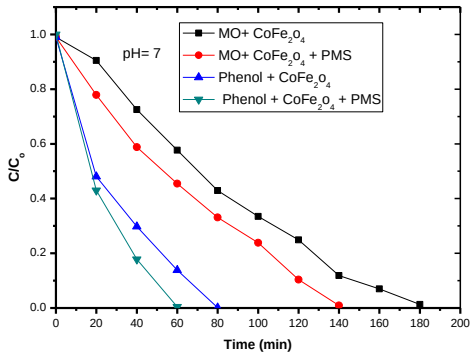

Fig. 9. Effect of pH 7 for the degradation of MO and Phenol

Effect of pH 10 on MO and Phenol

At pH 10, MO exist as a negatively charged ions, repulsion takes place between catalyst and surface of MO thereby activity decreases compared to phenolas shown in the Figure 10 and Table 4. Where phenol exist as negatively charged phenolate

$$Co^{2+} + H_2O \rightarrow CoOH^{+} + H^{+} \quad (8)$$

$$Co^{3+} + H_2O \rightarrow Co(OH)^{2+} + H^{+} \quad (9)$$

ion at this pH and phenolate ion exhibit acidic in nature, catalyst behaves as negative charge surface at the solution hence minimum repulsion takes place.

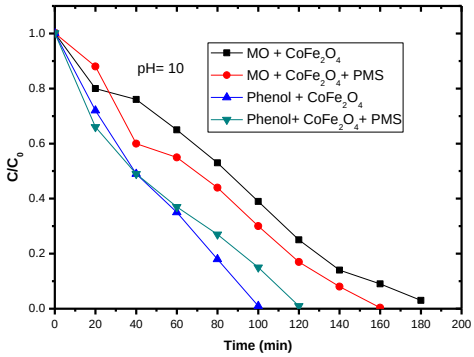

Fig. 10. Effect of pH 10 for the degradation of MO and Phenol

PMS plays very important role at pH 3, 7, 10. Under acidic conditions hydrogen bond between H^{+} and HSO^{-}_5 was dominated to inhibit the radical generation surface charge of $CoFe_2O_4$ was less attractive towards the PMS activation thereby shows less activity compared to pH 7. At pH 7, HSO^{-}_5 will be dominating species to interact with active sites on $CoFe_2O_4$ surface PMS exist as highly reactive species frequently generates sulphate radicals which are take part in the photocatalytic degradation process. PMS concentration was found to be most suitable for activation and could accelerate the reaction rate in the neutral medium. The cobalt ferrite with PMS generate freely diffusible hydroxyl and sulphate free radicals compared to cadmium ferrite with PMS may be due to the high surface area and Co^{3+} ion acts as electron pair donor. The rapid transferring of electron and high separation efficiency of electron-hole pairs are the main reason for the substantially enhanced photocatalytic activity at pH 7.

At pH 10, it is expected to decrease the phoyocatalytic activity coagulation of excess Co^{3+} ions takes place at higher pH conditions, inhibit the regeneration of Co^{2+} ions which are required for sustaining the photo cyclic reaction

However, at higher pH values PMS exists as less reactive dianion form (SO_5^{2-}). The efficient generation of $SO_4^{-\bullet}$takes place only from monoanion form (HSO_5^{-}) and its generation is almost insignificant from dianionform (SO_5^{2-}).

4. Conclusion

$CoFe_2O_4$ can be acts as charge collector to promote separation and transfer of photo generated carriers. Surface hydroxyls of Co^{2+}/PMS played an important role in the generation sulphate and hydroxyl free radicals both in MO and phenol at pH 7, PMS is active in neutral medium. In acidic and basic conditions sulphate and hydroxyl free radical ceases. Efficient photocatalytic activity shows towards phenol in presence of Co^{2+} /PMS at pH 7 due to its higher adsorption onto photocatalyst and surface was the active sites to catalyse phenol which confirms by the adsorptivity. Therefore, enhanced photocatalytic activity observed in case of phenol

References

[1] [X. Lou, J. Han, W. Chu, X. Wang, Q. Cheng, Synthesis and photocatalytic property of Co_3O_4 nanorods synthesis and photocatalytic property of Co_3O_4 nanorods, Mater. Sci. Eng.: B 137 (2007) 268–271.

[2] T.G. Xu, L. Zhang, W.H.Y. Cheng, Y.F. Zhu, Significantly enhanced photocatalytic performance of ZnO via graphene hybridization and the mechanism study, Appl Catal. B. 101 (2011) 382–387.

[3] B.H. Li, J. Cao, M. Shao, J.H. Qu, Warner, Synthesis of graphene@Fe_3O_4@C core shell nanosheets for high-performance lithium ion batteries, J. Mater. Chem. 21 (2011) 5069–5075.

[4] V. Hays, R, Marchand, G. Saindrenan and E.Garffet, Nanocrystalline Fe-Ni solid solutions prepared by mechanical alloying, Nanostructured Mater. 7 (4) (1996) 411-420,

[5] N. M. Deraz, "Production and Characterization of pure and doped copper ferrite nanoparticles," J. Analy. Appl. Pyrolysis, 82 (4) (2008) 212-222

[6] H. Yang, J, Z. Lu X. Cheng and Y. Tang, Photocatalytic activity evaluation of tetragonal $CuFe_2O_4$ nanoparticles for the H_2 evolution under visible light irradiation, J. alloys and comp., 476 (2009) 715-719

[7] A. Kezzim, N. Nasrallah, A Abdi and M. Trai Visible light induced hydrogen on the novel heterosystem $CuFe_2O_4/TiO_2$'' Energy conversion and Management 52 (2011) 2800-2806.

[8] Z. W. Wang, D. Schiferl, Y. S. Zhao, S. C. O. Neill, High Pressure Raman Spectroscopy of Spinel-Type Ferrite $ZnFe_2O_4$, J. Phys. Chem. Solids. 64, (2003) 2517–2523.

[9] C.G. Hatchard, C.A. Parker, A new sensitive chemical actinometer. I. Some trials with potassium ferrioxalate, Proceedings of the Royal Society Series A. 220 (1953) 104–15.

[10] R. Kavitha, L. Gomathi Devi, Synergistic effect between carbon dopant in titania lattice and surface carbonaceous species for enhancing the visible light photocatalysis, J. Environ. Chemi. Eng. 2 (2014) 857–867.

[11] Z. W. Wang, D. Schiferl, Y. S. Zhao, S. C. O. Neill, High Pressure Raman Spectroscopy of Spinel-Type Ferrite $ZnFe_2O_4$, J. Phys. Chem. Solids. 64, (2003) 2517–2523.

[12] K.H. Chan, W. Chu, Degradation of atrazine by cobalt mediated activation of peroxymonosulfate: different cobalt counter anions in

homogenous process and cobalt oxide catalysts in photolytic heterogeneous process, Water Res. 43 (2009) 2513–2521.
[13] L. Ai, H. Huang, Z. Chen, X. Wei, J. Jiang, Activated carbon/$CoFe_2O_4$ composites: facile synthesis, magnetic performance and their potential application for the removal of malachite green from water, Chem. Eng. J. 156 (2010) 243–249.
[14] X. Shu, J. He, D. Chen, Visible-light-induced photocatalyst based on nickel titanate nanoparticles, Ind. Eng. Chem. Res. 47 (2008) 4750–4753.
[15] S. Yanez-Vilar, M. Sanchez-Andujar, C. Gomez-Aguirre, J. Mira, M.A. Senaris-Rodriguez, S. Castro-Garcia, A simple solvothermal synthesis of MFe_2O_4 (M=Mn, Co and Ni) nanoparticles, J. Solid State Chem. 182 (2009) 2685–2690.
[16] X. Hui, J. Yan, Y. Xua, Y. Songa, L. Huaming, X. Jiexiang, C. Huang, H. Wan, Novel visible-light-driven AgX/graphite-like C_3N_4 (X=Br,I) hybrid materials with synergistic photocatalytic activity, Appl. Catal. B: Environ. 29 (2013) 182–193.
[17] X. Zhu, J. Liu, Z. Zhao, J. Yan, Y. Xu, Y. Song, H. Ji, X. Hui, L. Huaming, Hydrothermal synthesis of mpg-C3N4 and Bi_2WO_6 nest-like structure nanohybrids with enhanced visible light photocatalytic activities, RSC Adv. 7 (2017) 38682–38690.
[18] X. She, J. Wu, H. Xu, J. Zhong, Y. Wang, Y. Song, K. Nie, Y. Liu, Y. Yang, M.T.F. Rodrigues, R. Vajtai, J. Lou, D. Daolin, L. Huaming, P.M. Ajayan, High efficiency photocatalytic water splitting using 2D α-FeO/g-CN Z-scheme catalysts, Adv. Energy Mater. 7 (17) (2017) 1700025.